

Electron-phonon interaction in CdTe/CdMnTe/CdMgTe quantum wells

X. F. Wang

Centro Brasileiro de Pesquisas Físicas

Rua Xavier Sigaud 150

22290-180 Rio de Janeiro, RJ, Brazil and

Instituto de Física, Universidade do Estado do Rio de Janeiro

Rua São Francisco Xavier 524

20550-013 Rio de Janeiro, RJ, Brazil

I. C. da Cunha Lima

Instituto de Física, Universidade do Estado do Rio de Janeiro

Rua São Francisco Xavier 524

20550-013 Rio de Janeiro, RJ, Brazil

A. Troper

Centro Brasileiro de Pesquisas Físicas

Rua Xavier Sigaud 150

22290-180 Rio de Janeiro, RJ, Brazil and

Instituto de Física, Universidade do Estado do Rio de Janeiro

Rua São Francisco Xavier 524

20550-013 Rio de Janeiro, RJ, Brazil

(Draft —April 11, 2018)

The optic vibrational (confined and interface) modes and the electron-phonon and hole-phonon interactions are obtained, in dielectric continuum model, for two diluted magnetic semiconductor structures: a single well of $Cd_{1-x}Mn_xTe/Cd_{1-y}Mg_yTe$ with the magnetic ions in the well, and a double well of $CdTe/Cd_{1-x}Mn_xTe$, in which a thin layer of the magnetic material is grown in the middle of the structure. The scattering rates for the intra- and the inter-subband transitions are obtained for electrons and holes.

I. INTRODUCTION

During the recent years there has been increasing interest and considerable experimental and theoretical activity focused on the semimagnetic semiconductors, also called diluted magnetic semiconductors (DMS) [1,2]. These compounds have some unique properties leading to their potential use in a wide range of opto-electronic applications. Since 1977, when Kamarov *et al* [3] first reported the giant enhancement of magnetic-optical effects in $Cd_{1-x}Mn_xTe$, much effort has been directed towards the understanding of the physics underlying the unusual phenomena associated with these special semiconductors. As its non-magnetic counterpart, $Cd_{1-y}Mg_yTe$ has attracted much attention [4,5], due to their similarities in crystalline and electronic properties, and, as a consequence, the feasibility of the fabrication of structures such as quantum wells, quantum wires and dots [6]. For this reason, with the development of the technology of the molecular beam epitaxy, microstructures of DMS/non-magnetic semiconductors, built with the constituents $CdTe$, $Cd_{1-x}Mn_xTe$, $Cd_{1-y}Mg_yTe$, and the quaternary alloy $Cd_{1-x-y}Mn_xMg_yTe$, have been grown, and their magneto-optic properties have been largely explored. For instance, in structures built with a non-magnetic quantum well ($CdTe$) surrounded by DMS barriers, the magnetic tuning of the barrier potential induces important changes in the energy of the confined states, which appear as large Zeeman effects of the excitons in the quantum well [7,8]. Structures where the DMS layer ($CdMn$) Te is surrounded by non-magnetic material ($CdTe$ or $Cd_{1-y}Mg_yTe$) are also greatly interesting [9–11]. Therefore, it is worthwhile to understand in greater details the vibrational modes and the electron-phonon interaction in structures with these II-VI DMS. In particular, for the magneto-optic properties, as well as for the possible magnetic order, holes play an important role. We will give, in consequence, special attention to the hole-phonon interaction, considered here as being described by the same Frölich-like electron-phonon potential, calculated with the proper hole parameters. The lattice dynamics of the bulk $Cd_{1-y}Mn_yTe$ has been studied in detail, both experimentally and theoretically [12–14]. Basically, optical phonons always play an important role in determining many physical properties in those materials. Due to the confinement, Faraday rotation [9], Kerr effect [10], and RKKY interaction [15,16], as well as the optical vibrational modes, and the electron-phonon Fröhlich interaction may change greatly. At present, the effect of phonon confinement and its consequences on the electron-phonon interaction in polar semiconductor heterostructures seems to be reasonably understood [17,18]. In this paper, we will study the confinement effect on the carrier-optical-phonon interaction in two typical microstructures with a DMS thin film surrounded by non-magnetic material: a $CdTe/CdMnTe$ double well structure (in which case the $CdMnTe$ layer acts as a barrier), and a $CdMnTe/CdMgTe$ single quantum well (in which case the $CdMnTe$ layer is programmed to work as a well).

II. ELECTRON-OPTICAL-PHONON INTERACTION

According to the dielectric continuum model [17,19], the optical-phonon modes of small wavevector in a microstructure can be obtained by describing them in several layers with different dielectric functions. In each layer the dielectric function is expressed by the generalized Lyddane-Sachs-Teller relation, given in binary semiconductors by:

$$\varepsilon_1(\omega) = \varepsilon_{1\infty} \frac{(\omega^2 - \omega_{L1}^2)}{(\omega^2 - \omega_{T1}^2)}, \quad (1)$$

and, in ternary semiconductors:

$$\varepsilon_2(\omega) = \varepsilon_{2\infty} \frac{(\omega^2 - \omega_{L2\alpha}^2)}{(\omega^2 - \omega_{T2\alpha}^2)} \frac{(\omega^2 - \omega_{L2\beta}^2)}{(\omega^2 - \omega_{T2\beta}^2)}. \quad (2)$$

Here ω is the phonon frequency. The layers of different materials are denoted by numerical subscripts 1 or 2, the subscript L (T) indicating the bulk longitudinal (transverse) mode, and the subscripts α , β , etc, indicating different phonon branches in the bulk ternary alloy. $\varepsilon_{i\infty}$ is the high frequency dielectric constant of material $i = 1$, or 2. The optical phonon modes satisfy the classical electrostatic equations in each layer:

$$\nabla^2 \Phi(\mathbf{r}) = \frac{1}{\epsilon_0} \nabla \cdot \mathbf{P}(\mathbf{r}) \quad (3)$$

$$\mathbf{P}(\mathbf{r}) = \epsilon_0 \chi_i(\omega) \mathbf{E}(\mathbf{r}) \quad (4)$$

$$\mathbf{E}(\mathbf{r}) = -\nabla \Phi(\mathbf{r}), \quad (5)$$

where $\mathbf{P}(\mathbf{r})$ is the polarization field, $\mathbf{E}(\mathbf{r})$ is the electric field, and $\chi_i(\omega) = \epsilon_i(\omega) - 1$ is the dielectric susceptibility in layer i . The electric potential $\Phi(\mathbf{r})$ generated by the phonon modes, which interact with electrons through the Fröhlich coupling, and the normal component of electric displacement $\epsilon_i(\omega) d\Phi/dz$, are continuous at each interface [17]. The phonon modes are divided into two kinds. One kind is formed by the bulk-like modes, including the confined modes and the half space modes, the other kind is formed by the interface modes. The electric field induced by each phonon mode, is normalized *via* the integral [19] :

$$\int d\mathbf{r} |\nabla \Phi(\mathbf{r})|^2 \beta_i = \frac{\hbar \omega}{2 \epsilon_0}, \quad (6)$$

with $\beta_i = \frac{\omega}{2} \frac{\partial \epsilon_i}{\partial \omega}$. In planar microstructures, the electric potential has the form of $\Phi_{\vec{q}}(\mathbf{r}) = \frac{1}{\sqrt{S}} \phi_{\vec{q}}(z) e^{i\vec{q} \cdot \vec{r}}$, with \vec{q} being the phonon mode wavevector in the $x - y$ plane. $\phi_{\vec{q}}(z)$ is the phonon potential along the z -direction (growth direction), and its form depends on the structure architecture, and on the phonon mode.

The calculations are performed for the two structures. First, we consider a symmetric $CdTe/Cd_{1-x}Mn_xTe$ double well, as sketched in Fig. 1: two miniwells of width L are separated by a $Cd_{1-x}Mn_xTe$ barrier of width d . The potential of the barrier for electrons (holes) is the mismatch between the conduction (valence) band edges of $CdTe$ and $Cd_{1-x}Mn_xTe$. The electron (hole) wavefunction can be obtained by solving the Schrödinger equation in this structure assuming parabolic energy bands [20]. The second structure to be considered here is a single quantum well, consisting of a DMS layer of $Cd_{1-x}Mn_xTe$ (width L) inside a thick layer of $Cd_{1-y}Mg_yTe$. The concentrations, x and y are chosen in such way to make the non-magnetic layer work as a barrier for electrons and holes. The energy gap dependence on the Mn concentration x , and on the Mg concentration y , are given by [2,21,22]:

$$E_g(300\text{ K}) = (1.528 + 1.316x + 1.316y) \text{ eV} \quad (7)$$

$$E_g(10\text{ K}) = (1.595 + 1.607x + 1.592y) \text{ eV} \quad (8)$$

$$E_g(4.2\text{ K}) = (1.606 + 1.592x + 1.592y) \text{ eV} \quad (9)$$

Since the problem of a single well has been extensively discussed in the literature – the only particularity of the present calculation lying on the fact of the alloys taking the place of the pure binary compounds – for the sake of brevity, we will concentrate on the case of the double well, assuming that the interested reader can map it into the case of a single well easily [17].

In this double quantum well structure, the z -direction phonon potential $\phi_{\vec{q}}(z)$ can be classified into $CdTe$ confined modes, $CdMnTe$ confined modes, $CdMnTe$ half space modes, and interface modes. The former three kinds of phonon modes are the same as those in binary/binary double quantum wells [20], and will not be discussed here in detail, either.

A. The Interface phonon modes

There are six symmetric, and six anti-symmetric interface modes in a binary/ternary double quantum well. Their electric potentials $\Phi(\mathbf{r})$ have similar expressions:

1. Symmetric modes:

$$\phi_{\vec{q}s}^{IF}(z) = \begin{cases} D_s \cosh qz & \text{for } |z| < d/2 \\ B_s e^{-q|z|} + C_s e^{q|z|} & \text{for } d/2 < |z| < d/2 + L \\ A_s e^{-q|z|} & \text{for } d/2 + L < |z| \end{cases} \quad (10)$$

The frequencies of the symmetric interface modes are determined by the relation:

$$\begin{aligned} \varepsilon_1(\omega) \{ \varepsilon_1(\omega)(1 + e^{-qd}) \tanh(qL) + \varepsilon_2(\omega) \} + \\ \varepsilon_2(\omega) \{ \varepsilon_2(\omega)(1 - e^{-qd}) \tanh(qL) + \varepsilon_1(\omega) \} = 0 \end{aligned} \quad (11)$$

with

$$A_s = D_s e^{q(d/2+L)} [\cosh qL \cosh \frac{1}{2}qd + \frac{\varepsilon_2(\omega)}{\varepsilon_1(\omega)} \sinh qL \sinh \frac{1}{2}qd], \quad (12)$$

$$B_s = \frac{1}{2} D_s e^{qd/2} [\cosh \frac{1}{2}qd - \frac{\varepsilon_2(\omega)}{\varepsilon_1(\omega)} \sinh \frac{1}{2}qd], \quad (13)$$

and

$$C_s = \frac{1}{2} D_s e^{-qd/2} [\cosh \frac{1}{2}qd + \frac{\varepsilon_2(\omega)}{\varepsilon_1(\omega)} \sinh \frac{1}{2}qd], \quad (14)$$

where D_s is determined by the normalization relation:

$$S \frac{\partial \varepsilon_2}{\partial \omega} q [2A_s^2 e^{-q(2L+d)} + D_s^2 \sinh qd] + 2S \frac{\partial \varepsilon_1}{\partial \omega} q [B_s^2 e^{-qd} (1 - e^{-2qL}) + C_s^2 e^{qd} (e^{2qL} - 1)] = \frac{\hbar e^2}{\varepsilon_0} \quad (15)$$

2. Anti-symmetric modes:

$$\phi_{\vec{q}a}^{IF}(z) = \begin{cases} D_a \sinh qz & \text{for } |z| < d/2 \\ \pm B_a e^{-q|z|} \pm C_a e^{q|z|} & \text{for } d/2 < |z| < L + d/2 \\ \pm A_a e^{-q|z|} & \text{for } L + d/2 < |z| \end{cases}, \quad (16)$$

where the positive sign (+) is used for the range $z > 0$ and the negative sign (-) for the range $z < 0$. The frequencies of the anti-symmetric interface modes are determined by the relation:

$$\begin{aligned} \varepsilon_1(\omega) \{ \varepsilon_1(\omega)(1 - e^{-qd}) \tanh(qL) + \varepsilon_2(\omega) \} + \\ \varepsilon_2(\omega) \{ \varepsilon_2(\omega)(1 + e^{-qd}) \tanh(qL) + \varepsilon_1(\omega) \} = 0 \end{aligned} \quad (17)$$

with

$$A_a = D_a e^{qd/2+qL} [\cosh qL \sinh \frac{1}{2}qd + \frac{\varepsilon_2(\omega)}{\varepsilon_1(\omega)} \sinh qL \cosh \frac{1}{2}qd], \quad (18)$$

$$B_a = -\frac{1}{2} D_a e^{qd/2} [\frac{\varepsilon_2(\omega)}{\varepsilon_1(\omega)} \cosh \frac{1}{2}qd - \sinh \frac{1}{2}qd], \quad (19)$$

and

$$C_a = \frac{1}{2} D_a e^{-qd/2} [\frac{\varepsilon_2(\omega)}{\varepsilon_1(\omega)} \cosh \frac{1}{2}qd + \sinh \frac{1}{2}qd], \quad (20)$$

where D_a is determined by the normalization relation:

$$S \frac{\partial \varepsilon_2}{\partial \omega} q [2A_a^2 e^{-q(2L+d)} + D_a^2 \sinh qd] + 2S \frac{\partial \varepsilon_1}{\partial \omega} q [B_a^2 e^{-qd} (1 - e^{-2qL}) + C_a^2 e^{qd} (e^{2qL} - 1)] = \frac{\hbar e^2}{\varepsilon_0} \quad (21)$$

B. Scattering rates

With the electron (hole) wave functions $\psi_{n,\vec{k}}(z)$, and the phonon electric potentials $\phi_{\lambda,\vec{q}}(\mathbf{r})$, we can calculate the Fröhlich interaction

$$H_{e-p} = \sum_{n,n',\sigma} \sum_{\vec{k},\vec{q}} M(n, n', \vec{q}, q_z, \lambda) c_{n', \vec{k} + \vec{q}, \sigma}^\dagger c_{n, \vec{k}, \sigma} A_\lambda(\vec{q}), \quad (22)$$

where $A_\lambda(\vec{q}) = b_{\vec{q},\lambda} + b_{-\vec{q},\lambda}^\dagger$ is the phonon operator, and $M(n, n', \vec{q}, q_z, \lambda)$ is the Fröhlich interaction matrix in the structure:

$$M(n, n', \vec{q}, \lambda) = -e \int dz \psi_{n'}^*(z) \phi_{\lambda,\vec{q}}(z) \psi_n(z). \quad (23)$$

Here, n and n' are the indices of the electron subbands, and λ denotes the phonon branch, this latter including all other indices except the 2-D wavevector \vec{q} .

The zero-temperature scattering rate (inverse of the transition lifetime) for an electron in an initial state (n, \vec{k}) into a subband n' by emission of an optical phonon *via* the Fröhlich interaction, becomes:

$$\begin{aligned} \frac{1}{\tau(n, n', \vec{k})} &= W(n, n', \vec{k}) = 2\pi \sum_{\vec{k}', \vec{q}} \delta(E_f - E_i) \left| \langle n', \vec{k}', 1 | H_{e-p} | n, \vec{k}, 0 \rangle \right|^2 \\ &= \frac{1}{2\pi} \sum_{\lambda} \int_0^{\infty} k' dk' \int_0^{2\pi} d\theta \delta\left(\frac{k'^2}{2m_t^*} - \frac{k^2}{2m_t^*} - \omega_{\lambda}\right) |M(n, n', \vec{q}_0, \lambda)|^2, \end{aligned} \quad (24)$$

where the summation is extended to all final unoccupied states in the subband n' . Here \vec{k} (\vec{k}') is the 2D wavevector of the initial (final) state, $\vec{q}_0 = \vec{k}' - \vec{k}$, and θ is the angle between \vec{k} and \vec{k}' . m_t^* is the average transversal ($x - y$ plane) effective mass of the carrier [23].

III. RESULTS

The modified random-element isodisplacement (*MREI*) model [14,21,24] is employed to obtain the bulk vibrational modes in $Cd_{1-x}Mn_xTe$ and $Cd_{1-y}Mg_yTe$, with parameters given by Eunson Oh et al [21]. The corresponding dielectric functions *versus* the phonon energy for $CdTe$, $Cd_{0.5}Mn_{0.5}Te$ and $Cd_{0.1}Mg_{0.9}Te$ are shown in Fig. 2, according to Eqs. (1) and (2). In the following discussion, we use ω_{T1} (17.5 meV), and ω_{L1} (20.6 meV) to denote the phonon modes in bulk $CdTe$, ω_{T2C} , ω_{L2C} , ω_{T2M} , and ω_{L2M} to denote the phonon modes in bulk $CdMnTe$, and ω_{T3C} , ω_{L3C} , ω_{T3M} , and ω_{L3M} to denote the phonon modes in bulk $CdMgTe$, in sequence from lower to higher energy. Eq. (8) is used to estimate the barrier potential for electrons (70% of the energy gap mismatch) and holes (30% of the energy gap mismatch). The lowest two subbands for either electrons and holes are included, when calculating the scattering rates.

We consider, at first, the case of the $CdTe/CdMnTe$ double quantum well with $L = 50$ Å and $d = 10$ Å. In Fig. 3, we show the energy spectrum of the interface modes in $CdTe/Cd_{1-x}Mn_xTe$ double well with $x = 0.1, 0.5$, and 0.9 . Bulk samples of $Cd_{1-x}Mn_xTe$ have the zinc-blende structure only for $x \leq 0.7$. In MBE grown samples, however, the zinc-blende structure can be achieved even for $x = 1$. Eqs.(11) and (17) have solutions in the range of $\varepsilon_1/\varepsilon_2 \in [-1, 0)$ and $(-\infty, -1]$. Differently from a binary/binary double well, in a binary-ternary structure there are six symmetric, and six anti-symmetric interface modes, appearing in the ranges $[\omega_{T1}, \omega_{T2C}]$, $[\omega_{L2C}, \omega_{L1}]$, and $[\omega_{T2M}, \omega_{L2M}]$, respectively. At low Mn concentrations, ω_{T2C} , and ω_{L2C} are close to the phonon modes of $CdTe$, i.e., ω_{T1} and ω_{L1} . On the other hand, ω_{T2M} , and ω_{L2M} coincide with the localized mode associated to the Mn impurity in $CdTe$. For $x = 0.1$, we observe a small dispersion in the interface modes. In the other limit, when the concentration of Mn approaches $x = 1.0$, the frequencies of the phonon modes in bulk $Cd_{1-x}Mn_xTe$ approach the frequencies of the pure bulk $MnTe$, plus that of the Cd impurity mode. This results in the increase of the dispersion of the 3rd–6th (in order of increasing energy) interface modes. The dispersion of the 1st and the 2nd interface modes are small in all range of concentration. This happens because the frequency of the Cd impurity mode in $MnTe$ is almost the same as that of the transverse mode in $CdTe$.

In Fig. 4, we show the intra-subband and the inter-subband electron and hole scattering rates due to the emission of $CdTe$ confined phonon modes (grouped inside the circle C), as well as interface modes, as functions of the initial

electron kinetic energy for $x = 0.1, 0.5$, and 0.9 . The solid lines, the dashed lines, the dotted lines and the chained lines are the results corresponding to the transitions involving subbands $1 \rightarrow 1$, $2 \rightarrow 2$, $1 \rightarrow 2$, and $2 \rightarrow 1$, respectively. We observe a sudden change in the electron scattering rates due to the confined phonons as x goes from 0.1 to 0.5 . A saturation occurs after that concentration. The scattering rates for holes (due to confined phonons), on the other hand, are stronger than that for electrons (by a factor of 3, approximately, in large concentrations), and, differently from the electrons, are weakly dependent on x . The dependence of the scattering rates due to the interface modes on the magnetic ions concentration is, on the other hand, much weaker. Our results show, considering the order from low to high energy in Fig. 3, that only the 3rd to the 6th modes give significant scattering rates, both for electrons and holes. Only the symmetric modes contribute to the intra-subband transitions and only the anti-symmetric modes contribute to the inter-subband transitions. Our calculation, performed for each individual mode, shows also that, in the case of $x = 0.1$, the third symmetric interface mode dominates the intra-subband scattering rate, and the forth anti-symmetric interface mode dominates the inter-subband scattering rate. The 3rd, and the 6th symmetric modes generate almost the same scattering rates for the transition $1 \rightarrow 1$, and $2 \rightarrow 2$, but the 4th and the 5th symmetric modes give scattering rates for the transition $1 \rightarrow 1$, four times bigger than that for the transition $2 \rightarrow 2$. The scattering rates for the transitions $1 \rightarrow 2$ and $2 \rightarrow 1$, due to anti-symmetric interface modes, on the other hand, have almost the same values at definite initial kinetic energy. With the increase of the Mn concentration, the 5th and the 6th modes become more and more important. At $x = 0.5$, the 3rd, 4th, and 6th symmetric modes give important contributions for the intra-subband scattering. The same occurs for the 4th, 5th, and the 6th anti-symmetric modes, for the inter-subband scattering. In the case of holes, the most remarkable difference with the electron scattering rates is that the 4th interface phonon mode gives a greatly enhanced contribution. Besides, the hole scattering rate due to the 3rd and the 6th interface modes show an obvious increase with the increase of hole energy, for intra-subband transitions. Next, we consider the electron (hole) phonon interaction in a ternary/ternary $Cd_{1-x}Mn_xTe/Cd_{1-y}Mg_yTe$ single well, where the DMS layer works as a well (after the proper choice of $x < y$). The phonon modes in this structure can be obtained in the same way as that for a binary/binary single well [17], by just substituting the dielectric function of the binary compound (Eq. 1) the dielectric function of the ternary alloy (Eq. 2). The number of phonon modes in ternary/ternary single well is twice that in a binary/binary single well. In Fig. 5, the dispersion relations of the interface modes are shown for $Cd_{1-x}Mn_xTe/Cd_{1-y}Mg_yTe$, with two different compositions: (i) $x = 0.1$, $y = 0.5$, and (ii) $x = 0.5$, $y = 0.9$. The symmetric modes (solid lines) appears in the range $\varepsilon_2/\varepsilon_3 \in (-\infty, -1]$ and the anti-symmetric modes (dashed lines) in the range $\varepsilon_2/\varepsilon_3 \in [-1, 0)$. Observing the dashed line ($CdMnTe$) and the dotted line ($CdMgTe$) for dielectric function in Fig. 2, we observe that four symmetric and four anti-symmetric interface modes appear in the ranges $[\omega_{T2C}, \omega_{T3C}]$, $[\omega_{L3C}, \omega_{L2C}]$, $[\omega_{T2M}, \omega_{L2M}]$ and $[\omega_{T3M}, \omega_{L3M}]$.

The electron and hole scattering rates are shown in Fig. 6. According to our calculation for individual modes, in the case (i) the $CdTe$ -like modes give the major contribution among the confined modes. In the case (ii), the $MnTe$ -like modes dominate. The anti-symmetric interface modes give scattering rates ten times smaller than the symmetric modes. The contribution from the lowest energy interface mode is negligible comparing to other modes.

IV. COMMENTS

Our calculation is performed at $T=0$, and we have only considered the scattering assisted by the emission of optic modes. For that reason, in some cases, the scattering rate is zero below a certain energy threshold, corresponding to a minimum energy transfer equal to the energy of the lowest lying relevant optic vibrational mode. For the same reason, a saw-like structure may appear in the total scattering rates due to the emission of interface modes. The results obtained by using the parameters of the double well structure, shows no threshold for the $2 \rightarrow 1$ transition for electrons, because the energy difference between the bottom of the subbands is higher than the energy of the lowest lying relevant mode. A remarkable result, which is a consequence of the widths chosen for the wells and barrier, is that the interface modes dominate the electron scattering in the whole range of the magnetic ion concentration, whereas the confined modes dominate the low energy hole scattering in the intermediate and high magnetic ion concentration.

Contrarily to the case of the double well, in the ternary/ternary single well structure, for both choices of composition, there is just a weak dependence of the transition rates on the concentrations x and y . This is a consequence of the fact in structures those structures the barrier height did not change, because we took care of keeping the DMS material as the well. The differences on the scattering rates reflects, in this case, the changes on the optic phonon dispersion relations. As in the case of the double well structure, the scattering by interface phonons dominate the intra-subband electron transition. In what concerns the inter-subband, however, almost an order of magnitude weaker, it is hard to distinguish between the contributions due to the interfaces from those of the confined modes. We had to use arrows indicating each mode, in that case. For holes, above an initial kinetic energy just a few eV above the energy threshold, the intra-subband scattering rates are dominated by the interface modes, as in the case of electrons. However, the

inter-subband transitions are dominated by the confined phonons.

In summary, employing the *MREI* model to calculate the optical phonon modes in bulk ternary alloy $CdMnTe$ and $CdMgTe$, and, after that the dielectric function of those material in the energy range of $\sim 10meV$, we studied the confinement of optical phonon modes in binary/ternary double well and ternary/ternary single well structures within the framework of dielectric continuum model. Carrier scattering rates of emission of optical phonons in those structures are calculated.

ACKNOWLEDGMENTS

ICCL and XFW are grateful to C. Testelin for very fruitful discussions. This work was partially supported by FAPERJ and CNPq, in Brazil.

- [1] *Diluted Magnetic Semiconductors*, Mukesh Jain, World Scientific (1991).
- [2] J. K. Furdyna, and J. Kossut, in *Diluted Magnetic Semiconductors*, edited by J. K. Furdyna, and J. Kossut, Semiconductors and Semimetals, Vol. 24, edited by R. K. Willardson and A. C. Beer (Academic Press, N. Y., 1988).
- [3] A. V. Kamarov, S. M. Pjabchenko, O. V. Terletskii, I. I. Zheru and R. D. Ivanchuk, *Zh. eksp. teor. Fiz.* **73**, 608 (1977).
- [4] G. Reuscher, M. Keim, F. Fischer, A. Waag and G. Landwehr, *Phys. Rev. B* **53**, 16 414 (1996).
- [5] A. A. Sirenko, T. Ruf, M. Cardona, D. R. Yakovlev, W. Ossau, A. Waag and G. Landwehr, *Phys. Rev. B* **56**, 2124 (1997).
- [6] M. Illing, G. Bacher, A. Forchel, T. Litz, A. Waag and G. Landwehr, *Appl. Phys. Lett.* **66** 1815 (1995).
- [7] A. Wasiela, Y. Merle d'Aubigné, J. E. Nichols, D. E. Ashenford and B. Lunn, *Solid State Commun.* **76**, 263 (1990).
- [8] J. A. Gaj, W. Grieshaber, C. Bodin-Deshayes, J. Cibert, G. Feuillet, Y. Merle d'Aubigné and A. Wasiela, *Phys. Rev. B* **50**, 5512 (1994).
- [9] C. Buss, R. Frey, C. Flytzanis and J. Cibert, *Solid State Commun.* **94**, 543 (1995).
- [10] C. Testelin, C. Rigaux and J. Cibert, *Phys. Rev. B* **55**, 2360 (1997).
- [11] A. Lemaitre, C. Tetelin, C. Rigaux, S. Maćkowski, Nguyen The Kuoi, J. A. Gaj, G. Karczewski, T. Wojtowicz, and J. Kossut, *Phys. Rev. B* **57**, 4708 (1998).
- [12] M. Picquart, E. Amzallag, M. Balkanski, Ch. Julien, W. Gebicki and W. Nazarewicz, *Phys. Stat. Sol. (b)* **99**, 683 (1980).
- [13] S. Venugopalan, A. Petrou, R. R. Galazka, A. K. Ramdas and S. Rodriguez, *Phys. Rev. B* **25**, 2681 (1982).
- [14] D. L. Peterson, A. Petrou, W. Giriat, A. K. Ramdas and S. Rodriguez, *Phys. Rev. B* **33**, 1160 (1986).
- [15] T. Dietl, A. Haurry, and Y. Merle d'Aubigné, *Phys. Rev. B* **55**, R3347 (1997).
- [16] M. A. Boselli, I. C. da Cunha Lima and A. Ghazali, *J. Appl. Phys.* **85**, 6598 (1999).
- [17] N. Mori, T. Ando, *Phys. Rev. B* **40**, 6175 (1989); see also references therein.
- [18] R. Chen, D. L. Lin, and Thomas F. George, *Phys. Rev. B* **41**, 1435 (1990); D. L. Lin, R. Chen and Thomas F. George, *J. Phys.: Condens. Matter* **3**, 4645 (1991).
- [19] K. W. Kim and M. A. Stroscio, *J. Appl. Phys.* **68**, 6289 (1990).
- [20] X. F. Wang, I. C. da Cunha Lima and X. L. Lei, *Phys. Rev. B* **58**, 12 609 (1998).
- [21] Eunsen Oh, C. Parks, I. Miotkowski, M. Dean Sciacca, A. J. Mayur, and A. K. Ramdas, *Phys. Rev. B* **48**, 15 040 (1993).
- [22] T. Lebihen, E. Deleporte and C. Delalande, *Phys. Rev. B* **55**, 1724 (1997).
- [23] A. T. da Cunha Lima, I. C. da Cunha Lima and A. Ferreira da Silva, *Phys. Rev. B* **55**, 15 420 (1997).
- [24] L. Genzel, T. P. Martin and C. H. Perry, *Phys. Stat. Sol. B* **62**, 83 (1974).

FIG. 1. Schematic drawing of the $CdTe/Cd_{1-x}Mn_xTe$ double well structure.

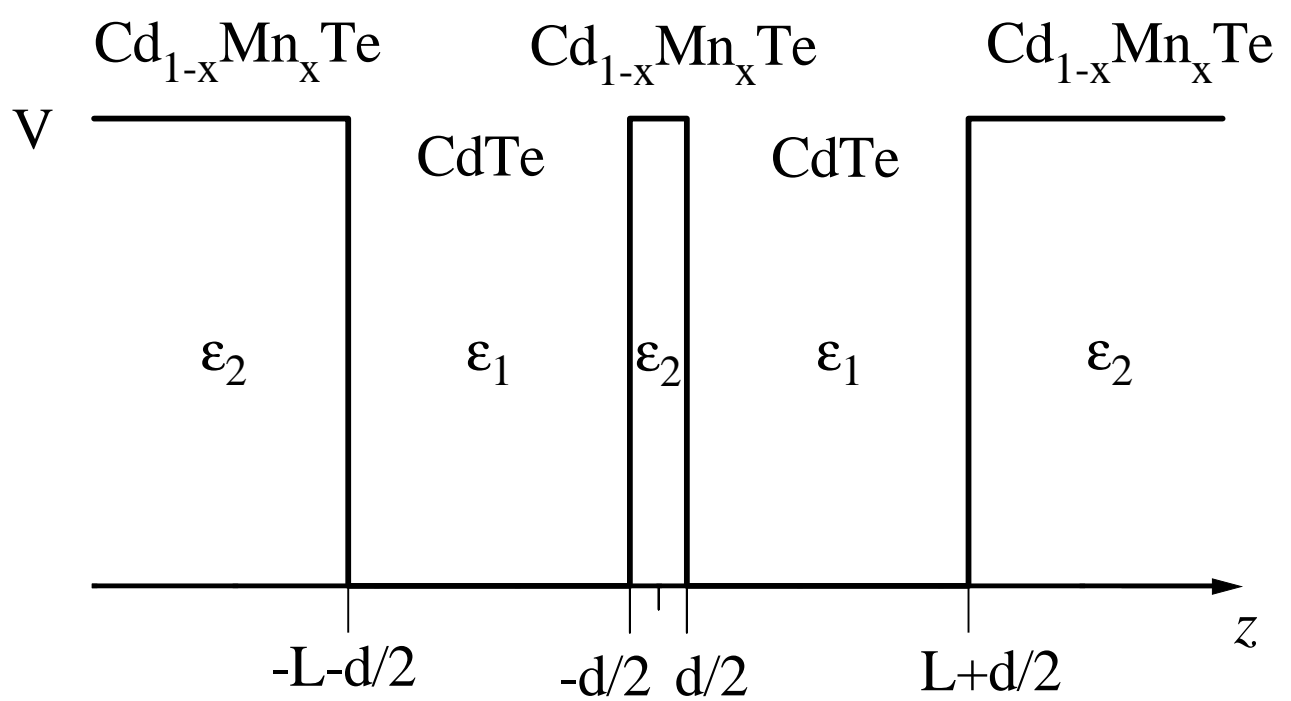
FIG. 2. Dielectric functions of $CdTe$ (solid line), $Cd_{0.5}Mn_{0.5}Te$ (dashed line), and $Cd_{0.1}Mg_{0.9}Te$ (dotted line), *versus* phonon energy.

FIG. 3. Energy spectra of the symmetric and anti-symmetric interface phonon modes in a $CdTe/Cd_{1-x}Mn_xTe$ double well with $x = 0.1$, $x = 0.5$ and $x = 0.9$.

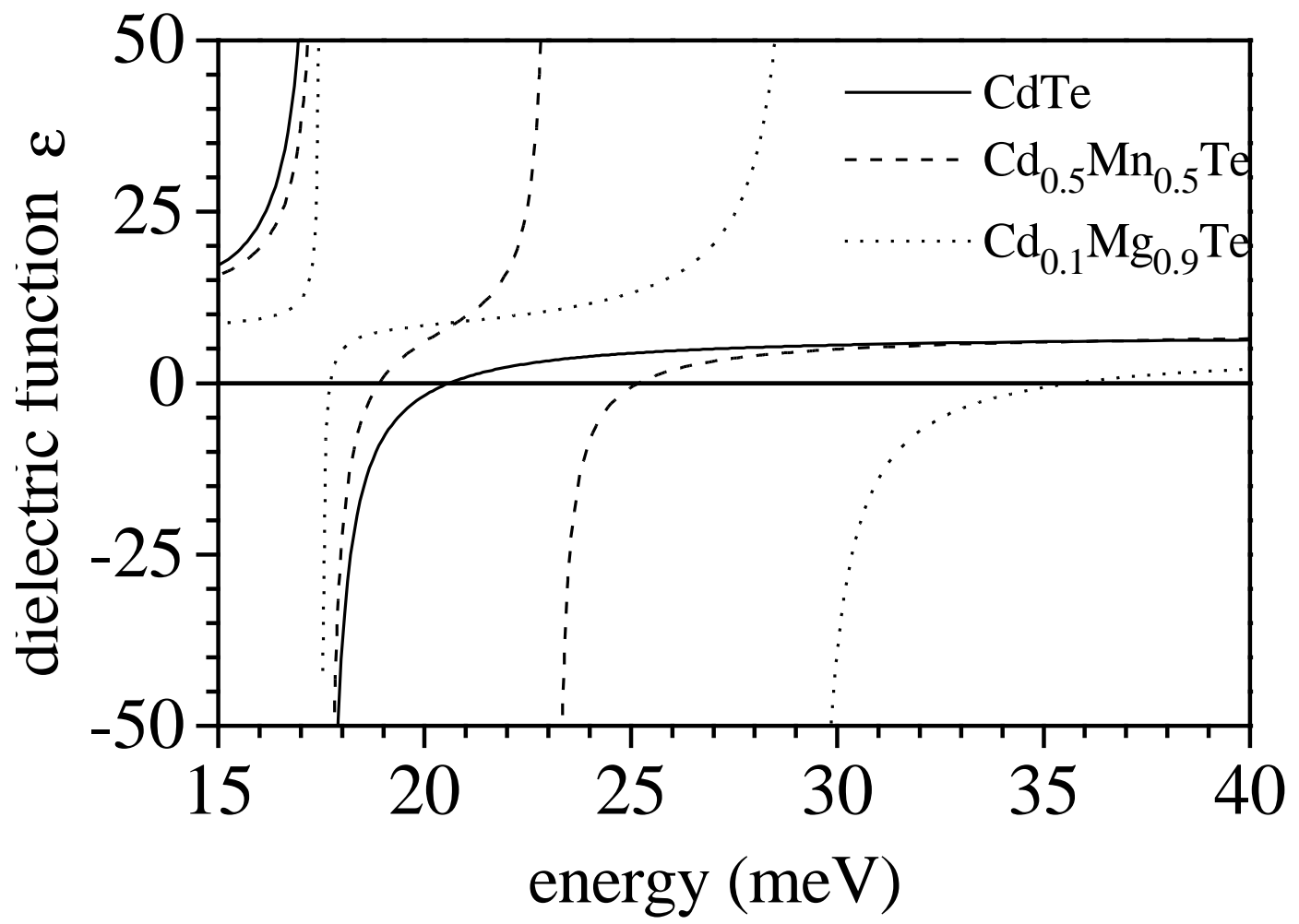
FIG. 4. Intra-subband (solid line for $1 \rightarrow 1$ and dashed line for $2 \rightarrow 2$) and inter-subband (dotted line for $1 \rightarrow 2$ and chained line for $2 \rightarrow 1$) scattering rates of the electrons and holes due to the emission of $CdTe$ confined phonons (grouped inside circle C), and of interface modes, as functions of the initial kinetic energy. The structure parameters are $L = 50 \text{ \AA}$ and $d = 10 \text{ \AA}$, with $x = 0.1$, $x = 0.5$ and $x = 0.9$.

FIG. 5. The symmetric (solid lines), and the anti-symmetric (dashed lines) interface phonon dispersion curves in a $Cd_{1-x}Mn_xTe/Cd_{1-y}Mg_yTe$ single quantum well of width $L = 50 \text{ \AA}$, and (a) $x = 0.1$, $y = 0.5$, (b) $x = 0.5$, $y = 0.9$.

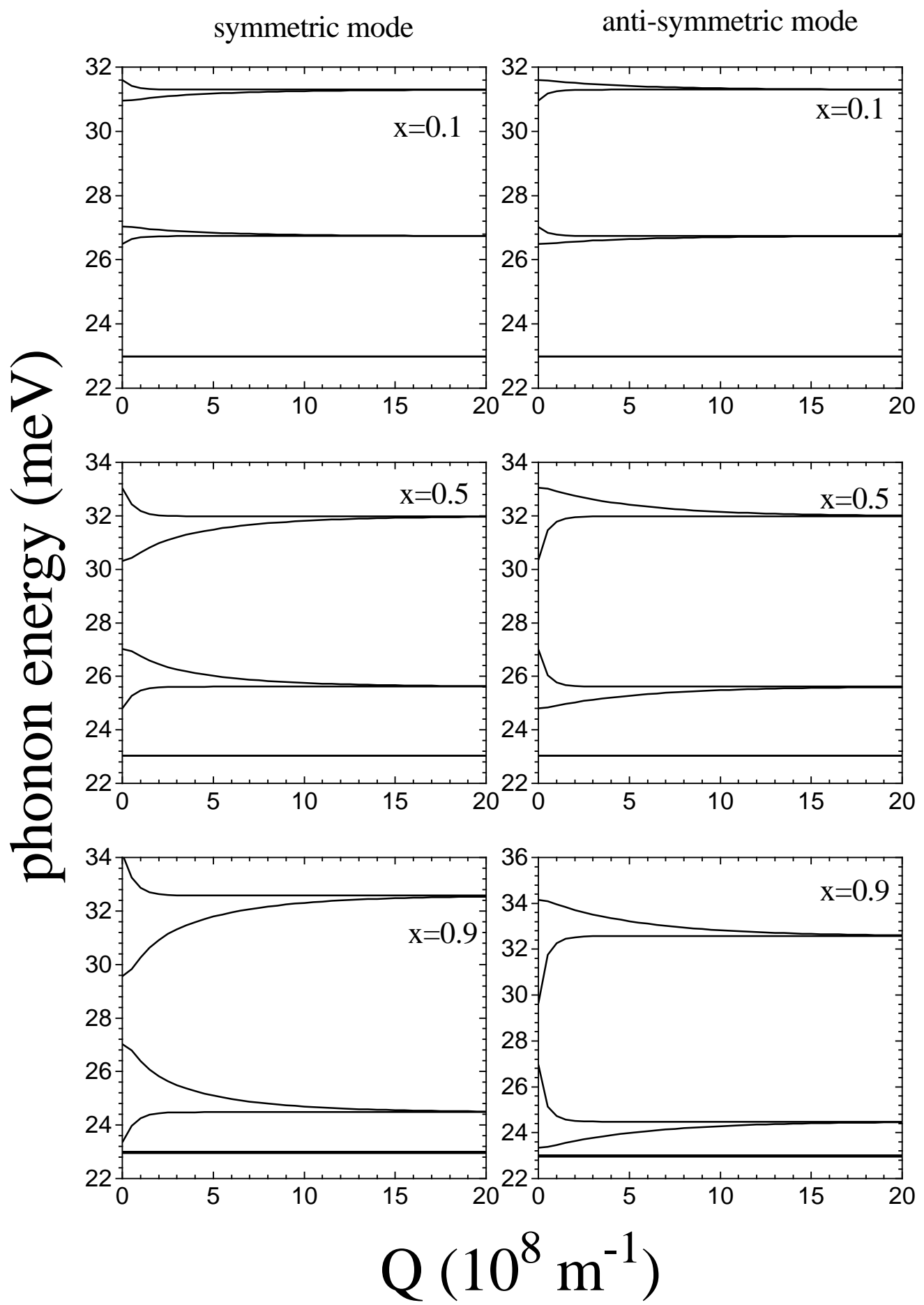
FIG. 6. Scattering rates due to emission of confined phonons (grouped inside circle C) and interface modes, as functions of the initial kinetic energy in the $Cd_{1-x}Mn_xTe/Cd_{1-y}Mg_yTe$ single well.



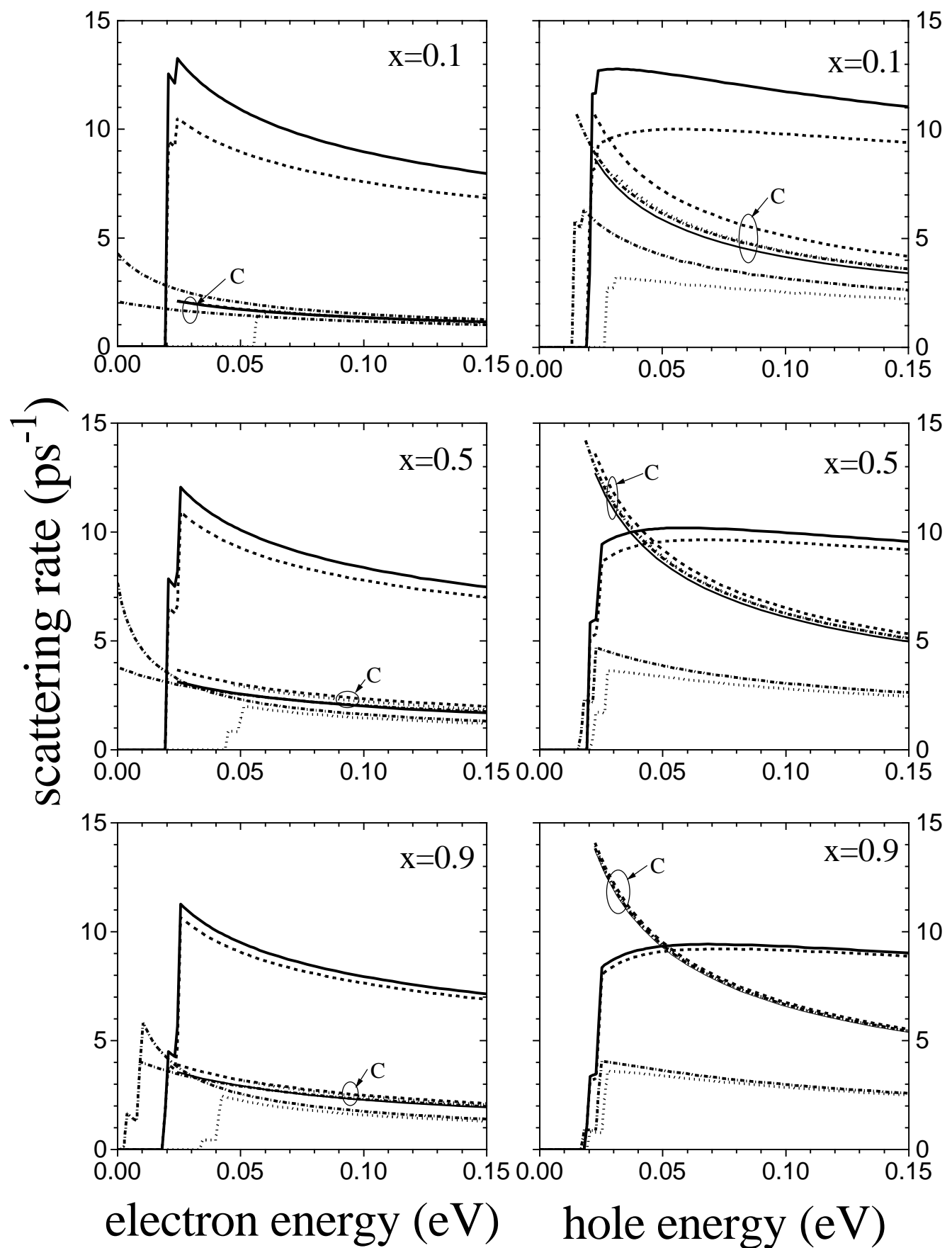
Wang, da Cunha Lima, Troper, Fig. 1



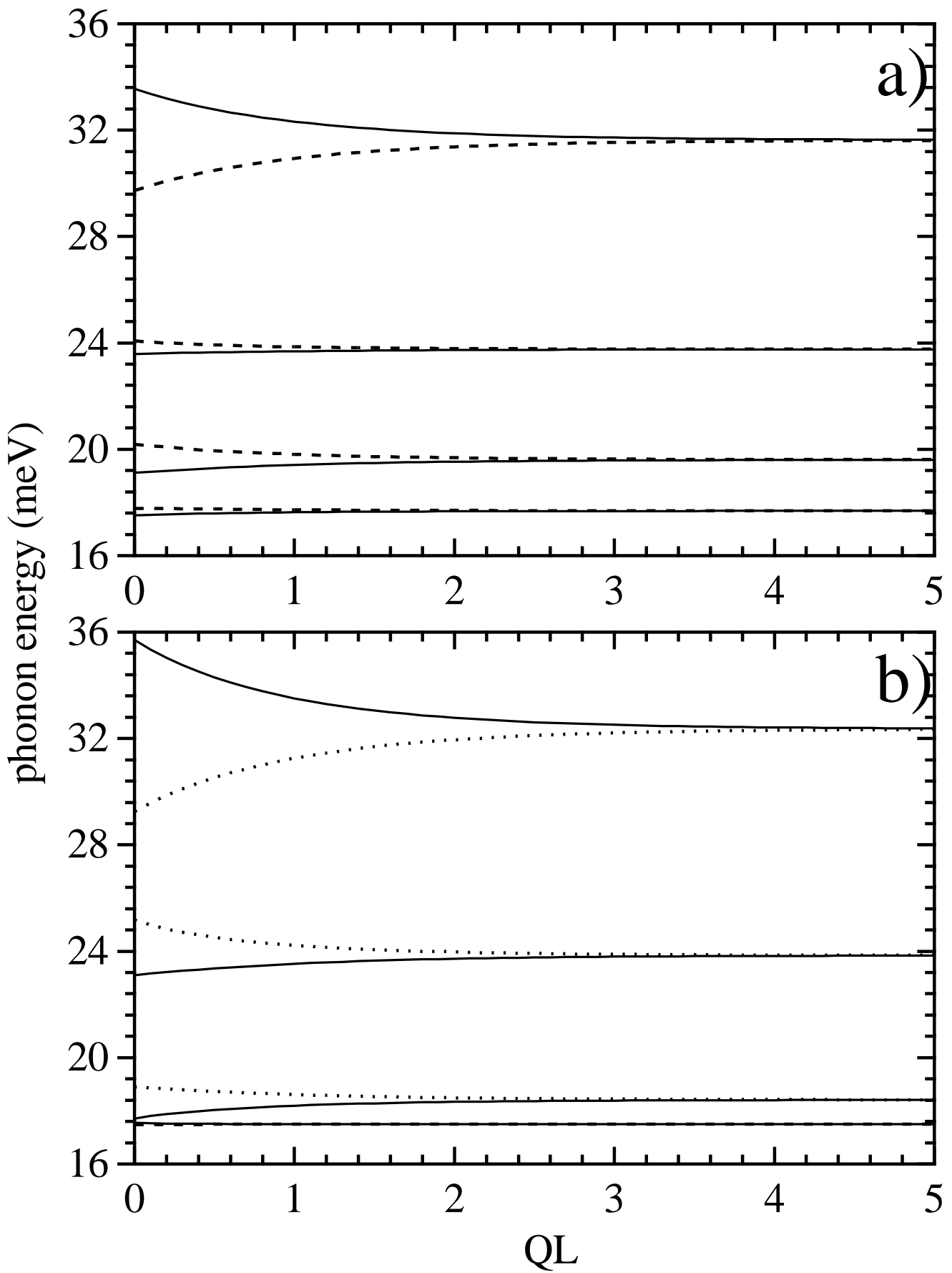
Wang, da Cunha Lima, Troper, Fig. 2



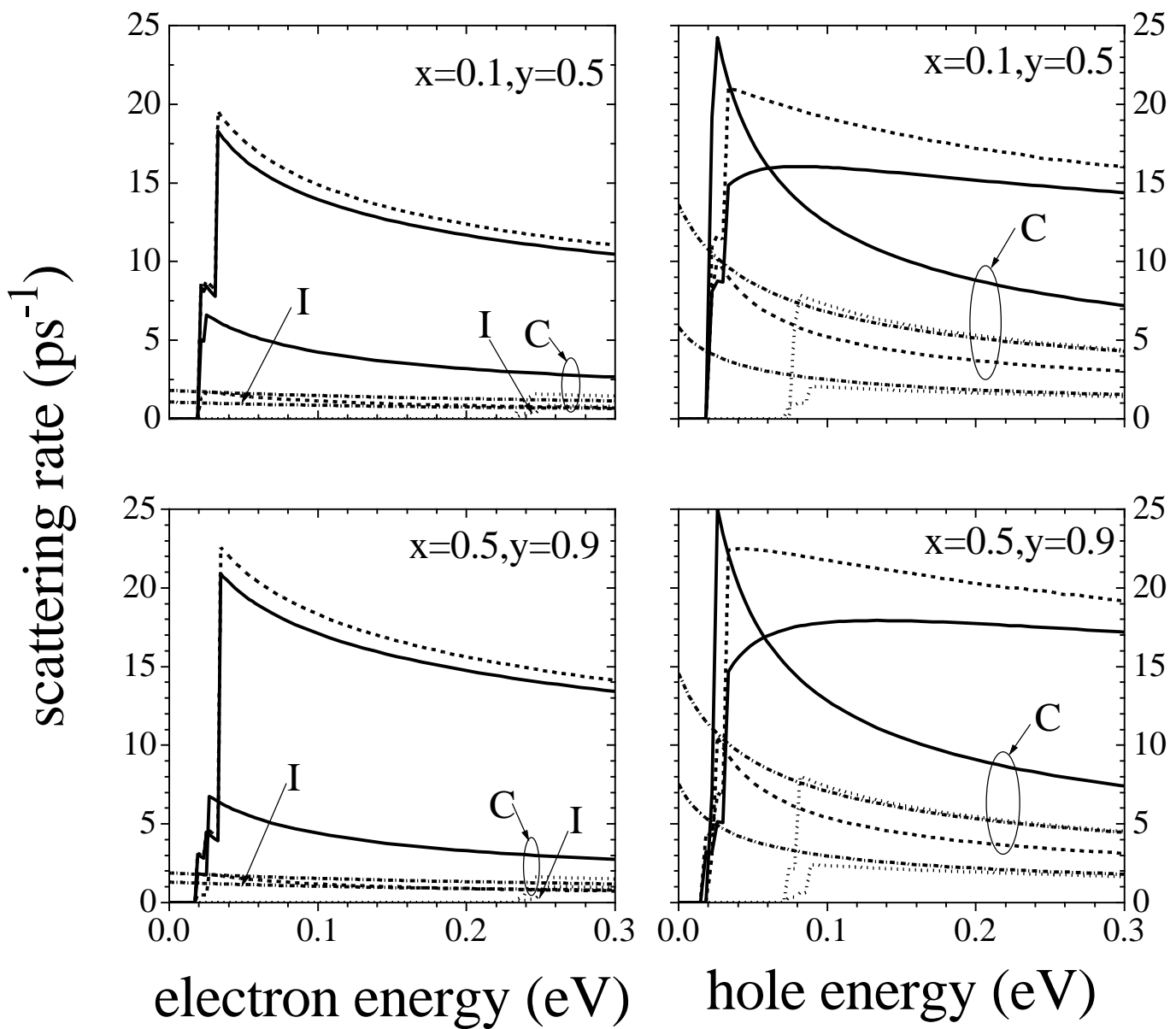
Wang, da Cunha Lima, Troper, Fig. 3



Wang, da Cunha Lima, Troper, Fig. 4



Wang, da Cunha Lima, Troper, Fig. 5



Wang, da Cunha Lima, Troper, Fig. 6